

Differentially private federated learning for localized control of infectious disease dynamics

Raouf Kerkouche¹, Henrik Zunker², Mario Fritz¹, Martin J. Kühn^{2,3}

1 CISPA Helmholtz Center for Information Security, Saarbrücken, Germany **2** Institute of Software Technology, Department of High-Performance Computing, German Aerospace Center, Cologne, Germany, **3** Bonn Center for Mathematical Life Sciences and Life and Medical Sciences Institute, University of Bonn, Bonn, Germany

 Shared first author. These authors contributed equally to this work.

* Martin.Kuehn@DLR.de

Abstract

In times of epidemics, swift reaction is necessary to mitigate epidemic spreading. For this reaction, localized approaches have several advantages, limiting necessary resources and reducing the impact of interventions on a larger scale. However, training a separate machine learning (ML) model on a local scale is often not feasible due to limited available data. Centralizing the data is also challenging because of its high sensitivity and privacy constraints. In this study, we consider a localized strategy based on the German counties and communities managed by the related local health authorities (LHA). For the preservation of privacy to not oppose the availability of detailed situational data, we propose a privacy-preserving forecasting method that can assist public health experts and decision makers. ML methods with federated learning (FL) train a shared model without centralizing raw data. Considering the counties, communities or LHAs as clients and finding a balance between utility and privacy, we study a FL framework with client-level differential privacy (DP). We train a shared multilayer perceptron on sliding windows of recent case counts to forecast the number of cases in the future, while clients exchange only norm-clipped updates and the server aggregated updates with DP noise. We evaluate the approach on COVID-19 data on county-level during two phases—November 2020 and March 2022 (Omicron). As expected, very strict privacy ($\epsilon \leq 0.5$) yields unstable, unusable forecasts. At a moderately strong but still privacy-preserving level ($\epsilon = 2$), the DP model closely approaches the non-DP model: $R^2 \approx 0.94$ (vs. 0.95) and mean absolute percentage error (MAPE) $\approx 26\%$ in November 2020; $R^2 \approx 0.88$ (vs. 0.93) and MAPE $\approx 21\%$ in March 2022. Overall, client-level DP-FL can deliver useful county-level predictions with strong privacy guarantees, and viable privacy budgets depend on epidemic phase, allowing privacy-compliant collaboration among health authorities for local forecasting.

Author summary

We address a practical challenge that many local health authorities face during fast accelerating outbreaks: they hold timely, sensitive case data that could improve short-term forecasts if they are used. However, legal and ethical constraints often prevent central sharing. We studied if several local health authorities (LHAs) can jointly train one central forecasting model while each LHA keeps its data entirely local.

Hereby, we build on federated learning (FL), where every site trains a shared neural network on its own recent case counts and only sends model updates. To further protect contributors, we apply differential privacy (DP), adding random noise so that no single participant’s information can be inferred from the final model. We test our approach on COVID-19 data published on county-level and for two different phases of the pandemic. We observe the expected tradeoff: very strict privacy settings destroy forecast quality, whereas moderately strong privacy-preservation approaches still yield trajectories close to a non-DP baseline. Our findings show that a privacy-preserving approach for regional infectious disease forecasting is feasible, and how an appropriate privacy level should be derived for different epidemic phases to maintain both usefulness and protection.

Introduction

In epidemic emergencies or situations of seasonally peaking endemic pathogens, public health experts and decision makers can benefit from predictions of infectious disease dynamics to proactively react to upcoming challenges. For prediction tasks, mechanistic mathematical models as well as ML models have proven to provide reliable outcomes. While for mechanistic metapopulation [1, 2], agent-based [3–5] or combined differential equation- and ML-based [6, 7] approaches, new situations might require the adaptations of existing mechanisms, many ML models are developed in a purely data-driven fashion, reducing the number of manual interventions cycles.

The traditional approach to training machine learning models typically requires centralizing data from multiple parties. This creates serious privacy risks when handling sensitive information such as medical records, which often cannot be shared directly. In infectious disease contexts, these records include precise dates of symptom onset and assumed transmission events, maintained by physicians, hospitals, or LHAs, and are critical for predicting future cases. While aggregation and anonymization can reduce exposure of sensitive information, they do not eliminate the risk of re-identification and often result in substantial information loss. Ensuring privacy-preserving approaches is therefore essential when working with such data.

To train ML models on spatially distributed data, FL has been introduced, enabling the collaborative training of a shared model without the need for data centralization [8–10]. FL allows each client to train the model on their own data and share only the model updates, or gradients, through a central server. The server aggregates these updates to improve the shared model, which is then redistributed to participants for further refinement. This process repeats until the model achieves satisfactory performance.

FL is grounded in three key objectives: First, it aims to protect the privacy of each participant’s data by exchanging model updates rather than the data itself. Second, it seeks to lower communication costs by allowing several local training iterations before the exchange of updates. Finally, by involving only a subset of clients in each round, it reduces communication overhead and increases resilience to the temporary unavailability of clients, offering particular advantages in scenarios with a large number of clients.

However, sharing gradients during collaborative learning can still reveal sensitive information from the training data of individual parties. Advanced attacks have demonstrated that adversaries can infer specific data records or group characteristics from intercepted model updates [11–17]. In extreme cases, they can reconstruct entire training samples from the gradients [16, 17]. Therefore, merely avoiding the sharing of actual training data can not completely avoid privacy leakage.

Initial works on calibrating noise to sensitivity [18] led to an extensive work of algorithmic foundations of *Differential Privacy* [19]. DP has emerged as a preeminent framework for enhancing data privacy, countering various privacy attacks associated

with FL. DP provides strong privacy assurances by ensuring that the behavior of the aggregated model does not depend significantly on any single client’s data. Instead, it captures commonalities across all contributions. Implementing DP involves adding Gaussian noise to the aggregated update, thereby masking participant data specifics while preserving the overall learning utility. In 2021, the authors of [20] had observed a substantial increase in the use of DP in health research publications and, among others, the authors of [21–24] developed a framework for privacy-preserving FL. In the context of the COVID-19 pandemic, the authors of [25] raised the awareness for a potential distortion of COVID-19 death rates when using DP with too small dataset groupings. During the COVID-19 pandemic, more than 1.9 million COVID-19 cases across Europe have been integrated in the DataSHIELD (Data Aggregation Through Anonymous Summary-statistics from Harmonised Individual-levEL Databases) platform [26], to allow for FL approaches to derive potential strategies against COVID-19 [27]. Among other things, DataSHIELD has already been used for other infectious diseases, e.g., to study malaria intervention in Mozambique [28].

In order to report dynamics and allow predictions by simultaneously addressing privacy concerns, COVID-19 case counts had been aggregated and reported on county-level throughout the pandemic in Germany [29]. We use these official aggregates as a proof-of-concept dataset to evaluate our method, which is intended for settings where finer-grained, potentially sensitive data remain with the LHAs. While aggregation reduces disclosure risk, it does not provide formal privacy guarantees [30]. In this study, we propose a differentially private federated learning approach designed to improve the prediction of new cases of a circulating pathogen, while providing theoretical guarantees for the protection of each participants information (client-level DP). While we validate our approach on published data on county-level, we suggest to explore the potential of localized predictions on a finer spatial scale when available.

Materials and methods

We develop a FL scheme with client-level DP to produce short-term local case forecasts while keeping raw data decentralized. Our goal is to develop a solution that ensures client-level privacy. For instance, in scenarios involving collaborative LHAs, our goal is to safeguard any information unique to each LHA’s training data. An adversary should not be capable of discerning from the received model or its updates whether any client’s data has been included in the federated run (within ϵ and δ bounds). DP provides plausible deniability not only for groups of a client’s samples but also for any client participating in the federated run. Consequently, any adverse privacy impact on clients (or their training samples) cannot be directly linked to their participation in the protocol run.

Data preprocessing

Our objective is time-series forecasting of local case counts using data which is reported on local level. We construct supervised learning examples by using a historical window of size $H = 10$ days over each administrative unit’s time series and predicting the case count $P = 7$ days ahead. Let $c_{k,t}$ denote the raw, unnormalized number of daily reported cases for geographic unit k , $k = 1, 2, 3, \dots$ on day t . Therefore, the input vector

$$\mathbf{x}_{k,t} = [c_{k,t-H+1}, \dots, c_{k,t}] \quad (1)$$

contains the reported daily cases on the preceding H days, and the target

$$y_{k,t} = c_{k,t+P} \quad (2)$$

is the case count P days into the future. Missing reports are handled as zero reported cases. From our dataset, we generate multiple input-label pairs for each administrative unit. Each input-label pair consists of an input window of H consecutive days and a target value P days ahead.

For model evaluation, we randomly select 10% of the generated input-label pairs as test set and the remaining 90% as training set. After splitting, we remove the location identifier from the feature vectors since they should not influence the model in any way.

Model architecture

We use PyTorch [31] to build a fully connected multilayer perceptron (MLP) as our prediction model. The architecture is consistent across both spatial resolutions, community- and county-based; see the *Results* section for details on the datasets used. The input to the network is a vector of length H containing the H most recent daily case counts; with zero reported cases counting as daily case count. This vector is propagated through three fully connected hidden layers of sizes 128, 64, and 32 neurons, each followed by a rectified linear unit (ReLU) activation function. A final linear output unit produce the predicted case count P days ahead. We use the mean squared error (MSE) as the loss function, which is minimized by the Adam optimizer with a learning rate of 0.001.

Differential privacy with federated learning

The core methodology employs FL with client-level DP, summarized in Algorithm 1. All hyperparameters are additionally explained in Table 1. The training process basically follows four steps:

1. **Client selection:** In each round t , a subset \mathbb{K} of clients is selected from the total number of clients N_{total} . Specifically, each client is independently included with probability

$$q = \frac{m}{N_{\text{total}}},$$

so that on average m participants (i.e., geographic units) contribute updates per round. This random sampling strategy reduces both communication and computational load. It also represents slow or unavailable clients, since each round depends only on the selected clients. When DP is enabled, this subsampling also amplifies privacy by lowering the effective per-round privacy loss.

2. **Local training:** Then, each selected client $k \in \mathbb{K}$ receives the current global model weights \mathbf{w}_{i-1} . The client then performs local training for a fixed number of epochs E on its own local dataset which remains local at all times. After local training completes, resulting in local model weights \mathbf{w}_{i-1}^k , the client k computes the local model update $\Delta \mathbf{w}_i^k = \mathbf{w}_{i-1}^k - \mathbf{w}_{i-1}$ relative to the initial given global model. Only this update is sent to the server, ensuring that no privacy critical data leaves the local client.
3. **DP mechanism:** When client-level DP is enabled (i.e., $\varepsilon < \infty$), each participating client first applies the Euclidean 2-norm bound on its model update $\Delta \mathbf{w}_i^k$ by clipping to a fixed sensitivity $S = 0.5$:

$$\Delta \widehat{\mathbf{w}}_i^k = \frac{\Delta \mathbf{w}_i^k}{\max(1, \|\Delta \mathbf{w}_i^k\|_2 / S)}.$$

The server then aggregates these clipped updates by summation and divides by the expected batch size m to obtain the mean update. Finally, Gaussian noise $\mathcal{N}(0, \sigma^2 \mathbf{I})$ is added to this averaged update, where

$$\sigma = \frac{S \cdot c}{m},$$

and the noise multiplier c is chosen via the Rényi DP (RDP) accountant [32]. If privacy is disabled ($\varepsilon = \infty$), no clipping or noise is applied and the raw updates $\Delta \mathbf{w}_i^k$ are simply averaged.

4. **Global model update:** Let

$$\Delta \bar{\mathbf{w}}_i := \frac{1}{m} \sum_{k \in \mathbb{K}} \Delta \hat{\mathbf{w}}_i^k$$

denote the mean clipped update. In the DP case, we draw $\xi_i \sim \mathcal{N}(0, \sigma^2 \mathbf{I})$. Then, the server updates the global model by adding the final averaged update:

$$\mathbf{w}_i = \mathbf{w}_{i-1} + \Delta \bar{\mathbf{w}}_i + \xi_i$$

In the non-DP case, this reduces to: $\mathbf{w}_i = \mathbf{w}_{i-1} + \Delta \bar{\mathbf{w}}_i$.

After T_{cl} rounds, the final global model is evaluated on the test dataset. To account for variability due to real random client selection and noise addition, the entire training steps are repeated multiple times with different random seeds.

Algorithm 1: Federated learning with client-level privacy.

```

1 Server:
2   Initialize common model  $\mathbf{w}_0$ 
3   for  $i = 1$  to  $T_{\text{cl}}$  do
4     Select a subset  $\mathbb{K}$  of clients randomly with probability  $q$ 
5     Initialize list of updates  $U = []$ 
6     for each client  $k \in \mathbb{K}$  do
7        $\Delta \hat{\mathbf{w}}_i^k = \mathbf{Client}_k(\mathbf{w}_{i-1})$ 
8       Insert  $\Delta \hat{\mathbf{w}}_i^k$  into  $U$ 
9     end
10     $\Delta \bar{\mathbf{w}}_i = \frac{1}{m} \sum_{\Delta \hat{\mathbf{w}} \in U} \Delta \hat{\mathbf{w}}$ 
11    if DP enabled then
12      Calculate noise multiplier  $c$  using an RDP accountant for  $(\varepsilon, \delta, q, T_{\text{cl}}, E)$ 
13       $\sigma = (S \cdot c) / m$ 
14      Draw  $\xi_i \sim \mathcal{N}(0, \sigma^2 \mathbf{I})$ 
15       $\mathbf{w}_i = \mathbf{w}_{i-1} + \Delta \bar{\mathbf{w}}_i + \xi_i$ 
16    else
17       $\mathbf{w}_i = \mathbf{w}_{i-1} + \Delta \bar{\mathbf{w}}_i$ 
18    end
19  end
20 Client $_k$ ( $\mathbf{w}_{i-1}$ ):
21    $\tilde{\mathbf{w}}_i = \mathbf{w}_{i-1}$ 
22   Train  $\tilde{\mathbf{w}}_i$  on local data  $D_k$  for  $E$  epochs using Adam ( $\eta = 0.001$ )
23    $\Delta \mathbf{w}_i^k = \tilde{\mathbf{w}}_i - \mathbf{w}_{i-1}$ 
24    $\Delta \hat{\mathbf{w}}_i^k = \Delta \mathbf{w}_i^k / \max\left(1, \frac{\|\Delta \mathbf{w}_i^k\|_2}{S}\right)$ 
25   Output:  $\Delta \hat{\mathbf{w}}_i^k$ 

```

Table 1. Overview of model hyperparameters

Symbol	Description
H	Input window length (days)
P	Prediction horizon (days)
E	Number of local training epochs per round
m	Predefined expected number of clients selected per round (expected batch size)
T_{cl}	Total number of FL rounds
q	Probability of selecting each client per round
S	Euclidean 2-norm clipping bound for each update
c	Noise multiplier for DP Gaussian mechanism
ε	DP budget
δ	Privacy failure probability
η	Learning rate (Adam)

Results

In this section, we provide results of our DP-FL approach applied to county-level data and discuss potential extensions and preliminary results for finer resolved data.

Dataset

We use official reported county-level COVID-19 case data from the LHAs transferred to the Robert Koch Institute (RKI) [29] and accessed via the *memilio-epidata* Python package [33]. We consider two different pandemic stages, first, late-stage as of March 2022 and, second, early stage as of November 2020. For each county and day, we obtain the newly confirmed infections plus estimated recoveries and deaths reported with the (assumed) day of infection. This data covers all 400 German counties. While the published data is stratified on county-level, the counties can, again, be divided by communities, summing up to a total of 10,786 communities in Germany. In Fig 1, Panel A, shows the population distribution across the counties, highlighting the variation in population sizes. The median county population is 147,524, while the mean population is 200,525, as several counties have a substantial larger population. The largest county by population has 3,685,265 inhabitants (Berlin, after merging all Berlin districts), and the total population across all counties is approximately 83.6 million. This heterogeneity in county sizes presents a particular challenge for our FL approach. Counties with larger populations typically report higher absolute case numbers. In addition, we show in Panel B the distribution of population sizes on community-level.

Synthetic community data

To examine whether predictive performance is maintained on finer levels and to evaluate robustness, we generated synthetic case datasets on community-level in Germany. In Fig 1, we show the distribution of population sizes for community and county sizes. While the median county population is 147,524 as of 2022, the median community population is 1,832; see [34].

To generate a community-based dataset, we sampled randomly from the county-based dataset, using weights given by community population divided by the corresponding county population. For the spatial stratification and an exemplary result for the county of "Coesfeld", see Fig 2, Panel B. In the resulting dataset, zeros were imputed for days when no case data was sampled for the particular community.

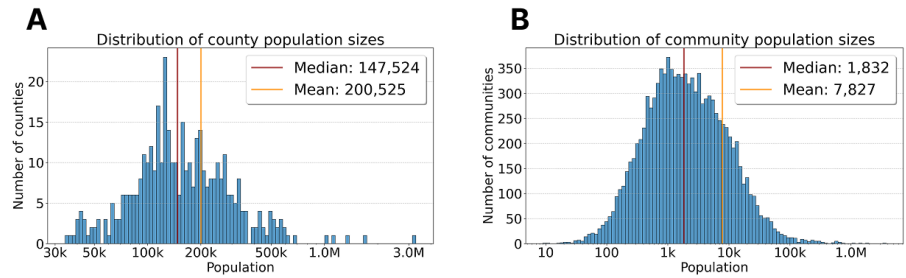


Fig 1. Distribution of population sizes on community and county-level. Panel A shows the distribution of county population sizes across all 400 German counties, with a median population of 147,524 and mean population of 200,525. Panel B displays the distribution of community population sizes across the 10,786 communities included in our analysis, with a substantially smaller median population of 1,832 and mean of 7,827. Red and orange vertical lines indicate median and mean values, respectively.

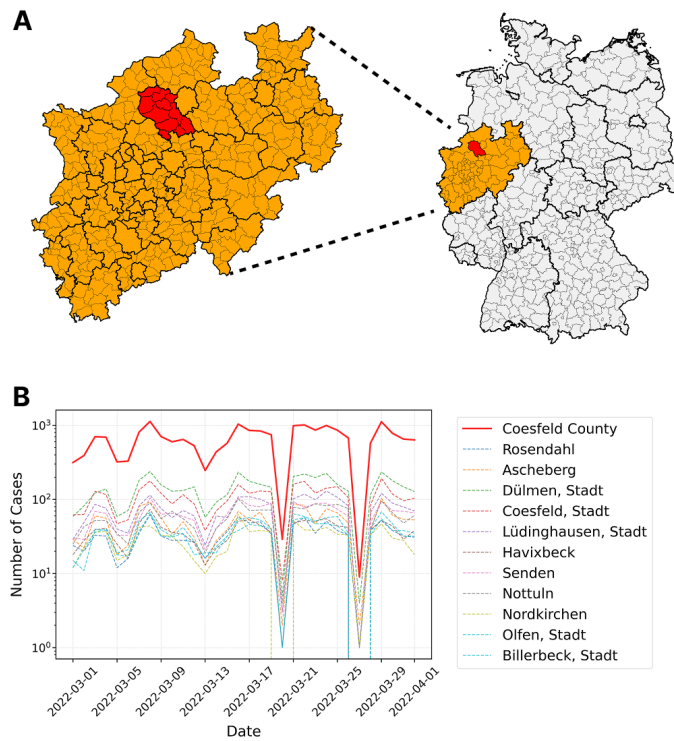


Fig 2. Spatial resolution of German counties and communities and community-based case data. Panel A presents two maps shown side by side. The left map presents North Rhine-Westphalia (NRW) stratified into counties (thick black boundaries) and communities (thin gray boundaries), highlighting county "Coesfeld" in red. The right map displays the stratification of Germany into federal states (thick black boundaries) and counties (thin gray boundaries), highlighting the federal state NRW in orange. Panel B shows the obtained community-based dataset for "Coesfeld" for March 2022, with the county-level aggregate shown in red and individual community trajectories in various colors. The left map from Panel A is using geodata "Verwaltungsgebiete 1:250 000 Stand 01.01. (VG250 01.01.)" from <https://gdz.bkg.bund.de>, copyright; GeoBasis-DE / BKG 2021, license dl-de/by-2-0, see <https://www.govdata.de/dl-de/by-2-0>.

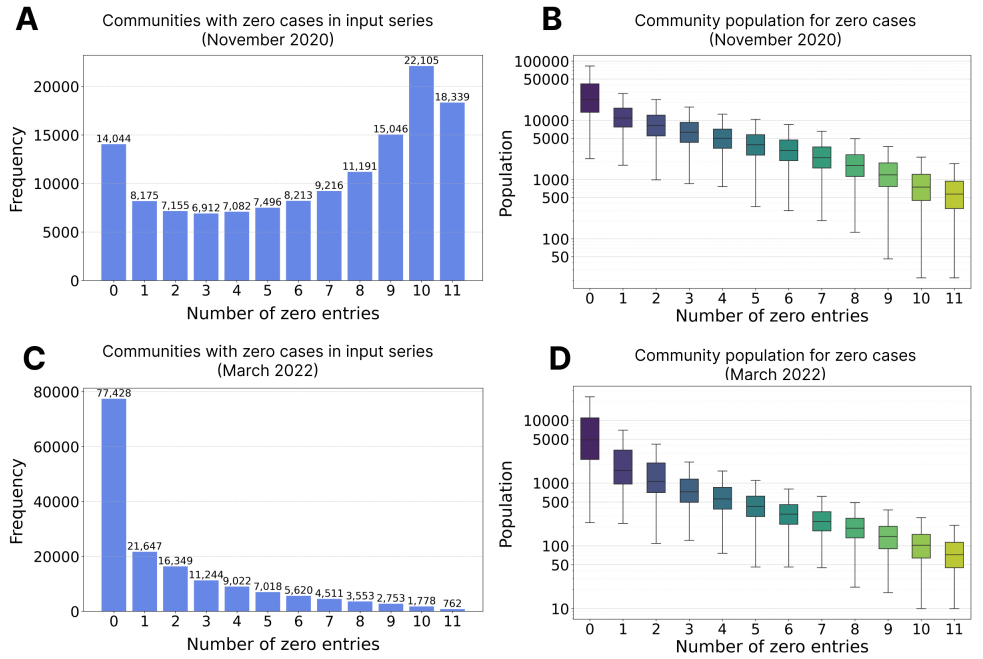


Fig 3. Communities with zero cases on input horizon and prediction day. Panel A shows the number of communities with 0 to 11 zero entries in the considered time series for November 2020 and Panel B shows the size of the community populations with the corresponding number of zeros. Panel C and D report the same structure for March 2022.

Based on this synthetic dataset, we applied our DP-FL approach. Instead of reporting the results directly, which measured in MAPE or R^2 looked much better than they actually were, we provide preliminary analyses on the outcomes. In particular, when DP was used (noise added to the aggregated, clipped updates), we did not observe deteriorated predictions, a precautionary signal.

In Fig 3, we provide the number of communities with zero confirmed cases over the input horizon $H = 10$ days plus the one prediction day; cf. Eqs. (1) and (2). While we see that for March 2022 much less communities have a high number of zero entries, the approach showed similar problems for both periods. With the application of a 7-day centered moving average, we substantially reduced the number of zero entries but did not obtain a dataset for which we observed substantially different results. That means, we did not observe a prediction deterioration when the noise increased with $\varepsilon \rightarrow 0.3$. We suspect that this outcome is an artifact due to two properties. In the synthetically created dataset, we obtain either relatively many zero entries for a large number of community's time series or very small entries in the case of a moving average applied. In addition, the random sampling for the community dataset could have yielded time series which were already highly noisy such that the addition of DP noise did not qualitatively change the time series pattern to be learned. In order for FL and DP to be validated on community-level, we conclude that additional experiments will be necessary and that access to a true community-based dataset will be required.

Published county data

As county-level case data was the finest resolved data available, we validate our approach on this level. In Fig 4, Panels A and C, we see the total infection dynamics in

Germany with clearly visible waves of infection during early 2022 and late 2020. These Panels also demonstrate the typical weekly reporting pattern observed in the data, with pronounced drops in reported cases during weekends followed by increases during weekdays. To mitigate these reporting artifacts, we applied a centered 7-day moving average to the daily case counts, resulting in smoother time series as shown by the orange line.

In Fig 4, Panels B and C, we present the geographical distribution of COVID-19 cases across the German counties. We see that the local entities have their own infection dynamics and that waves are partly desynchronized.

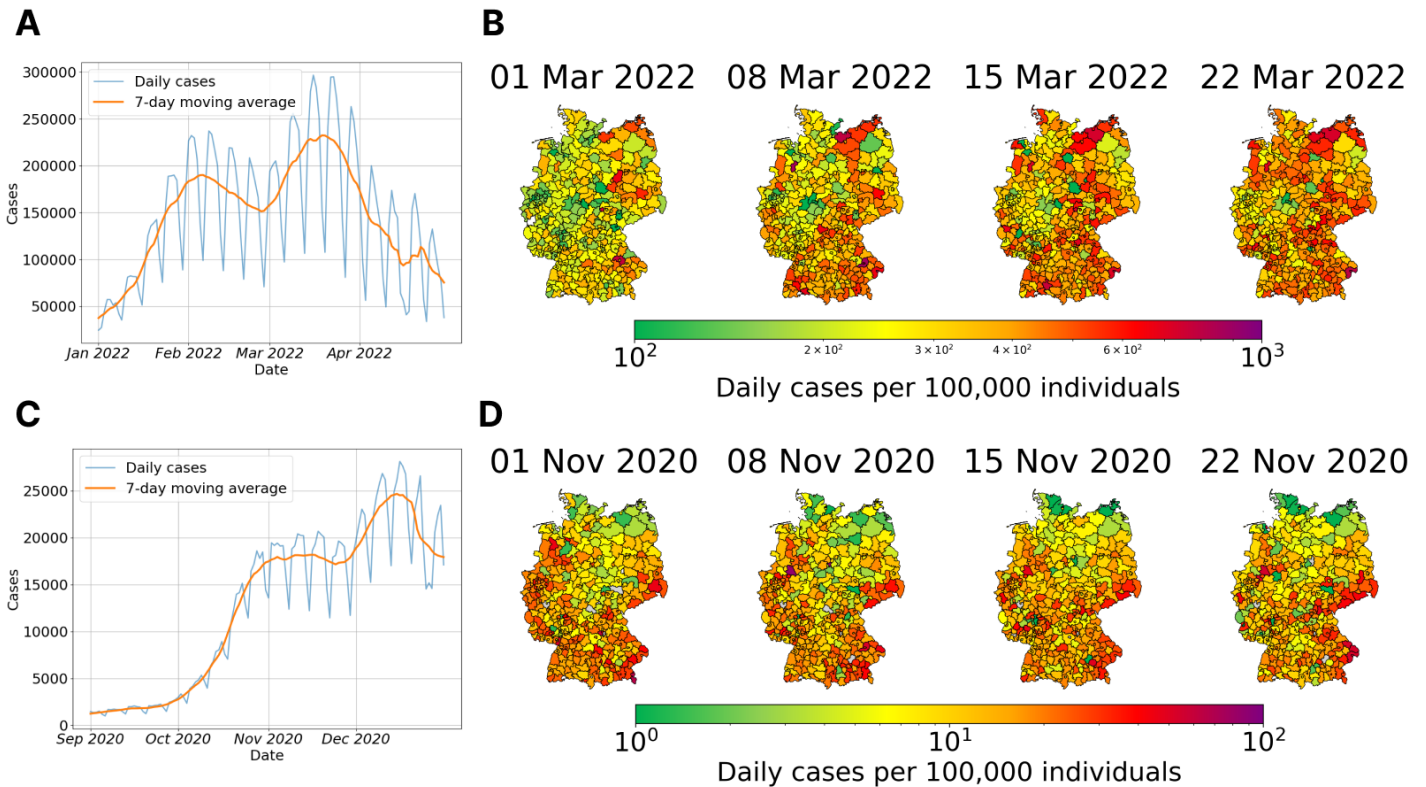


Fig 4. Analysis of COVID-19 case numbers in Germany on county-level. Panel A presents the time series of daily new infections throughout early 2022, showing both raw daily counts (blue) and the 7-day moving average (orange) that smooths the weekly reporting pattern. Panel B plots the geographical distribution of the COVID-19 incidence per 100,000 population at four weekly intervals in March 2022, illustrating the spatial heterogeneity of infection patterns and their temporal evolution. Panel C and D show the same type of data for late 2020.

County-level prediction March 2022

First, we evaluated our FL approach on county-level COVID-19 case data from March 2022, which represents a challenging period during the Omicron wave characterized by high peaks and dynamic infection trajectories. In Table 2 and Fig 5, we present the performance metrics across different privacy budget levels, ranging from strict privacy guarantees ($\epsilon = 0.3$) to no differential privacy ($\epsilon = \infty$, non-DP).

Table 2. Performance metrics for COVID-19 case prediction on March 2022 data. Results from 15 runs, 75 federated rounds, and 30 local epochs per round for different privacy budget levels. The metrics include Mean Squared Error (MSE), Mean Absolute Error (MAE), Mean Absolute Percentage Error (MAPE), and R^2 score. All values are reported as mean \pm standard deviation across runs.

ϵ	MSE	MAE	MAPE (%)	R^2
0.3	$1.26 \times 10^{10} \pm 1.65 \times 10^{10}$	$6.80 \times 10^4 \pm 4.69 \times 10^4$	$1.33 \times 10^4 \pm 9.02 \times 10^3$	$-4.82 \times 10^4 \pm 6.28 \times 10^4$
0.5	$2.99 \times 10^8 \pm 3.98 \times 10^8$	$9.97 \times 10^3 \pm 8.17 \times 10^3$	$1.96 \times 10^3 \pm 1.60 \times 10^3$	$-1.14 \times 10^3 \pm 1.52 \times 10^3$
1.0	$4.00 \times 10^5 \pm 5.71 \times 10^5$	349.55 ± 299.23	68.80 ± 58.75	-0.53 ± 2.18
2.0	$3.13 \times 10^4 \pm 2.37 \times 10^4$	105.29 ± 38.35	20.75 ± 6.30	0.88 ± 0.09
non-DP	$1.91 \times 10^4 \pm 1.54 \times 10^3$	81.42 ± 3.16	16.36 ± 0.51	0.93 ± 0.01

Our results demonstrate a clear privacy-utility tradeoff that is characteristic of DP implementations. As shown in Fig 5, the quality of predictions declines substantially as we strengthen the privacy guarantees, i.e., by decreasing the privacy budget ϵ . In particular, for $\epsilon = 0.3$ and $\epsilon = 0.5$ the models are effectively unusable as the predictions showing no correlation with the true case counts (see Panel A and B in Fig 5). At the strictest privacy level ($\epsilon = 0.3$), the model produced predictions that were almost completely unrelated to the actual values, with an extremely high MSE of 1.26×10^{10} and a strongly negative R^2 value of approximately -48208 . The mean absolute percentage error (MAPE) was over 13,000%, which makes the complete failure of the predictive ability even more clear. Also, the standard deviation of these metrics across the runs is of the same order of magnitude or larger than the mean values themselves, indicating extreme instability in the prediction behavior. At $\epsilon = 0.5$, while still poor, the model begins to show marginal improvement, with MSE reduced by about two orders of magnitude to 2.99×10^8 . However, the predictions remain basically unusable with MAPE near 2,000% and R^2 still deeply negative at approximately -1140 . Fig 5(B) shows that while there is slightly more structure to the predictions, they still fail to track the true values in any meaningful way. A substantial qualitative improvement emerges at $\epsilon = 1.0$, where the MSE drops to around 400,000, and MAPE decreases to approximately 69%. While the R^2 value remains slightly negative at -0.53 , indicating the model still performs worse than a simple mean predictor, the predictions begin to show some correlation with the true values, as proven in Fig 5(C). At $\epsilon = 2.0$, we observe that the model achieves positive predictive value, with an R^2 of 0.88. Despite the privacy, the overall performance is comparable to the non-DP case. The MAPE decreases to around 21%, and the predictions visibly track the true values as shown in Fig 5(D). The non-private (non-DP) model shows our performance ceiling with the highest R^2 value of 0.93 and the lowest MAPE at 16.36%. Fig 5(E) demonstrates the most accurate tracking of true values.

Beyond the mean performance metrics, the standard deviations across runs reveal important insights about the stability of differentially private models. As ϵ decreases, the standard deviations increase dramatically, reflecting the noise introduced by the privacy mechanism. This is especially evident in Fig 5(F), which shows box plots of the MAPE calculated for each individual county predictions. For these box plots, the individual MAPE values for each county from all runs were collected and then visualized separately for each privacy level. Each box plot thus represents the distribution of prediction errors across all counties and runs for a given privacy level.

The substantial outliers for $\epsilon = 0.3$ and $\epsilon = 0.5$ illustrate the extreme variability in model performance at these privacy levels, whereas the non-DP and $\epsilon = 2.0$ cases show much more consistent performance.

These results highlight that for our dataset, there appears to be a minimum viable privacy budget (approximately $\epsilon = 1.0$) below which predictions become too unreliable

for practical use. However, the model at $\epsilon = 2.0$ demonstrates that it is possible to nearly match the performance of a non-DP model while still providing strong privacy guarantees. This suggests that when designing privacy-preserving prediction systems for infectious disease dynamics, the balance of privacy requirements against the need for reliable predictions must be carefully considered.

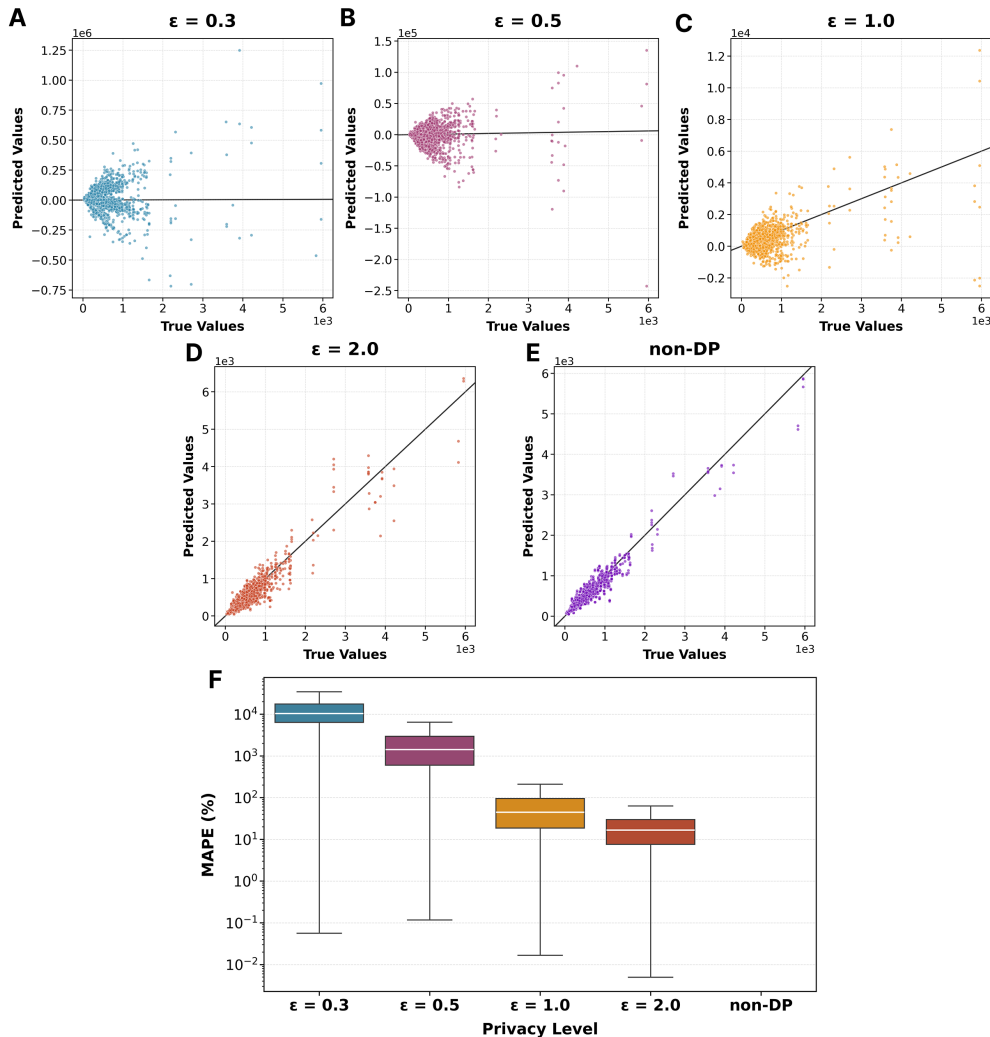


Fig 5. Comparison of prediction performance across different privacy levels for March 2022 data. Panels A-E show scatter plots of predicted against true case counts for various privacy budgets: (A) $\epsilon = 0.3$, (B) $\epsilon = 0.5$, (C) $\epsilon = 1.0$, (D) $\epsilon = 2.0$, and (E) $\epsilon = \infty$ (non-DP). The black diagonal line represents perfect prediction. Panel F displays box plots of Mean Absolute Percentage Error (MAPE) for individual county predictions across all runs and privacy levels, illustrating the decreasing error and variance as privacy budget increases.

County-level prediction November 2020

In addition, we evaluate our model's performance and the DP tradeoff for an earlier stage of the pandemic as of November 2020. The November 2020 data evaluation reveals patterns consistent with those observed in the 2022 dataset, but with several notable differences that highlight how pandemic phase and disease dynamics influence the effectiveness of privacy-preserving predictive models. The metrics for the 2020 data

are summarized in Table 3 and show a similar trend as the 2022 data in Table 2.

Similar to the 2022 results, we observe a clear degradation in model performance as the privacy budget decreases. At $\epsilon = 0.3$, the model again produces essentially unusable predictions with extremely high MSE (2.03×10^8) and deeply negative R^2 values (approximately -45940). The MAPE values exceed 13,700%, indicating complete prediction failure. As shown in Fig 6(A), predictions at this privacy level appear randomly distributed with no correlation to actual case counts. At $\epsilon = 0.5$, while still performing poorly, the model shows considerably better metrics than the equivalent privacy level in the 2022 data. The MSE drops to approximately 1.8 million, which represents a reduction of about two orders of magnitude compared to the 2022 results at the same privacy level (2.99×10^8). The MAPE also shows relative improvement at 1,356% versus 1,964% in the 2022 data. At $\epsilon = 1.0$, the model achieves near-zero R^2 (-0.01), indicating performance approximately equivalent to a mean-value predictor. This is substantially better than the corresponding 2022 model at the same privacy level ($R^2 = -0.53$). The MSE improves to 4,480, compared to nearly 400,000 in the 2022 data. Fig 6(C) shows predictions that begin to correlate with true values, but still with considerable dispersion. At $\epsilon = 2.0$, the model achieves good performance with $R^2 = 0.94$, nearly matching the non-DP model. The MAE of 9.37 is only marginally higher than the non-DP value of 8.52, suggesting that at this privacy level, the added noise has minimal impact on practical prediction quality. Fig 6(D) shows predictions that closely track the actual values across the entire range of case counts. The non-DP model establishes a slightly higher performance ceiling than in the 2022 data, with $R^2 = 0.95$ compared to 0.93. Also, the absolute errors are substantially lower in the 2020 data, with MAE of 8.52 against 81.42 in 2022, reflecting the lower absolute case numbers during this earlier pandemic phase. However, the MAPE is actually higher at 24.97% versus 16.36% in 2022, suggesting that despite lower absolute errors, the relative prediction accuracy may be somewhat worse.

The variance in model performance across multiple runs, as reflected in the standard deviations, follows similar patterns to the 2022 data, with extreme variability at low privacy budgets that stabilizes as ϵ increases. Fig 6(F) illustrates this through the MAPE box plots, which shows the distribution of individual percentage errors (MAPE) for each county across all runs. These box plots highlight the substantial outliers and wide distributions at $\epsilon = 0.3$ and $\epsilon = 0.5$ that contract substantially at higher privacy budgets.

In summary, the results for 2020 confirm the results from the 2022 data. Again, we were able to achieve good prediction performance at $\epsilon = 2.0$, with the model closely matching the non-DP case but still preserving privacy guarantees.

Table 3. Performance metrics for COVID-19 case prediction on November 2020 data. Results from 15 runs, 75 federated rounds, and 30 local epochs per round.

ϵ	MSE	MAE	MAPE (%)	R^2
0.3	$2.03 \times 10^8 \pm 2.91 \times 10^8$	$5.77 \times 10^3 \pm 5.00 \times 10^3$	$1.37 \times 10^4 \pm 1.14 \times 10^4$	$-4.59 \times 10^4 \pm 6.58 \times 10^4$
0.5	$1.80 \times 10^6 \pm 2.53 \times 10^6$	566.38 ± 454.17	$1.36 \times 10^3 \pm 1.07 \times 10^3$	-406.51 ± 574.01
1.0	$4.48 \times 10^3 \pm 4.36 \times 10^3$	30.84 ± 16.44	72.28 ± 34.87	-0.01 ± 0.99
2.0	282.48 ± 108.03	9.37 ± 1.37	25.95 ± 3.40	0.94 ± 0.02
non-DP	213.14 ± 4.55	8.52 ± 0.11	24.97 ± 0.55	0.95 ± 0.01

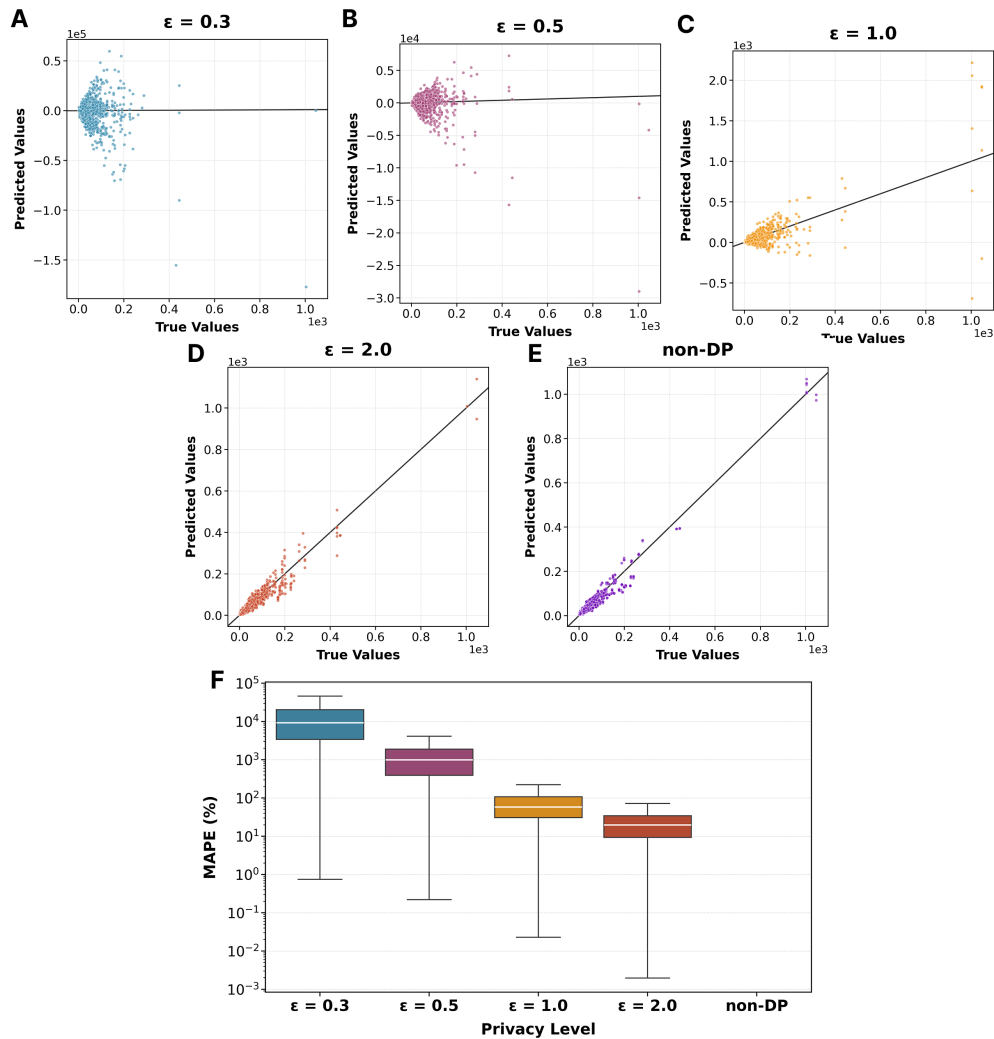


Fig 6. Comparison of prediction performance across different privacy levels for November 2020 data. Similar to Figure 5, Panels A-E show scatter plots of predicted versus true case counts for various privacy budgets, while Panel F displays box plots of MAPE for individual county predictions across all runs.

Discussion

We developed a differential privacy-preserving federated learning approach for predicting COVID-19 case numbers on a spatially resolved level and validated the approach on county-level for two different time periods, November 2020 and March 2022. This was done to explore the balance between prediction accuracy and privacy-preservation in different stages of the pandemic. Our results demonstrate a clear relationship between privacy level (expressed through the privacy budget ϵ) and prediction quality.

One goal of our study was to explore the possibility of localized predictions at a finer spatial resolution than the county-level. Although we developed a probabilistic approach to disaggregate county data to the community-level, the resulting data proved inadequately representative of actual local dynamics. The random assignment of cases to communities based on population data led to datasets that are unrealistic, particularly for small communities, and potentially do not reflect actual epidemic spread. This experience underscores the challenges of working with sensitive health data

at a highly resolved spatial level. While protecting privacy is a key concern, the availability of granular data is crucial for precise localized predictions. Due to the lack of case data resolved on community-level with often only several hundreds of individuals, we could not test our approach on very small population units. Future research will thus consider the creation of a more realistic synthetic dataset. This dataset should follow the structural patterns as observed during the COVID-19 pandemic on community-level. Furthermore, it should be created such that it can be published for scientific research. To do so, we will reach out to public health experts with access to more finely resolved data series.

Our findings on county-level confirm the fundamental tradeoff between privacy and utility that is characteristic of differential privacy implementations. At very strict privacy guarantees ($\epsilon = 0.3$ and $\epsilon = 0.5$), predictions are practically unusable, as evidenced by extremely high MSE values and negative R^2 values. This observation aligns with the theoretical foundation of differential privacy, where a lower ϵ value leads to stronger noise addition to model parameters.

For a privacy-preserving budget of $\epsilon = 2.0$, we were able to achieve predictions that closely match the quality of non-DP models, with an R^2 value of 0.88 for the 2022 data and 0.94 for the 2020 data. The MAPE was around 21% for the 2022 data and 25.95% for the 2020 data, indicating that while there is some degradation in prediction quality compared to non-DP models, the results are still practically useful. This suggests that with a carefully chosen privacy budget, it is possible to achieve a good balance between privacy protection and prediction accuracy.

A limitation of our study concerns the quality and resolution of the underlying data. Clearly, it would have been better if we could also have validated our approach on the much smaller communities. Besides that we attempted to mitigate weekend effects by applying a 7-day moving average, these partially remain and limit the models learning ability. Eventually, problem of underreporting prevails: the reported case numbers represent only a fraction of actual infections with differences in spatial levels. According to data from the Robert Koch Institute [29], test positivity rates in 2022 ranged between 30% and 50%, indicating a substantial number of unreported cases. This underreporting affects the prediction quality, especially if the extent of underreporting varies temporally and spatially.

The tradeoff between the need for detailed data for precise predictions and privacy requirements underscores the relevance of our FL approach with DP, which can enable LHAs to use their granular data for collaborative learning without directly sharing it.

As an important outcome for public health, we conclude that with an appropriate privacy budget ($\epsilon = 2.0$), DP-FL models can generate predictions that nearly match the quality of non-DP models. This opens up possibilities for privacy-compliant collaboration between LHAs without heavily affecting the quality of decision support. However, it should be noted that privacy budgets might need dynamic adaptation to the epidemic situation.

Overall, our work demonstrates that privacy-preserving federated learning approaches are suitable in principle for predicting infectious disease dynamics if the privacy budget is carefully chosen.

Acknowledgments

This work was supported by the Initiative and Networking Fund of the Helmholtz Association (grant agreement number KA1-Co-08, Project LOKI-Pandemics).

Competing interests

The authors declare to not have any competing interests.

Data availability

All data used in this study are publicly available from the Robert Koch Institute (RKI) and can be accessed via the *memilio-epidata* Python package [33]. The code used to generate the results of this study is available at <https://github.com/SciCompMod/memilio-simulations>.

Author Contributions

Conceptualization: All authors

Data Curation: Henrik Zunker, Raouf Kerkouche

Formal Analysis: Henrik Zunker, Raouf Kerkouche, Martin Kühn

Funding Acquisition: Mario Fritz, Martin Kühn

Investigation: Henrik Zunker, Raouf Kerkouche, Martin Kühn

Methodology: All authors

Project Administration: Mario Fritz, Martin Kühn

Resources: Mario Fritz, Martin Kühn

Software: Henrik Zunker, Raouf Kerkouche

Supervision: Mario Fritz, Martin Kühn

Validation: All authors

Visualization: Henrik Zunker

Writing – Original Draft: Henrik Zunker, Raouf Kerkouche

Writing – Review & Editing: All authors

References

1. Zunker H, Schmieding R, Kerkmann D, Schengen A, Diexer S, Mikolajczyk R, et al. Novel travel time aware metapopulation models and multi-layer waning immunity for late-phase epidemic and endemic scenarios. *PLOS Computational Biology*. 2024;20(12). doi:10.1371/journal.pcbi.1012630.
2. Zunker H, Dönges P, Lenz P, Contreras S, Kühn MJ. Risk-mediated dynamic regulation of effective contacts de-synchronizes outbreaks in metapopulation epidemic models. *Chaos, Solitons & Fractals*. 2025;199:116782. doi:10.1016/j.chaos.2025.116782.
3. Kerr CC, Stuart RM, Mistry D, Abeysuriya RG, Rosenfeld K, Hart GR, et al. Covasim: An agent-based model of COVID-19 dynamics and interventions. *PLOS Computational Biology*. 2021;17(7):1–32. doi:10.1371/journal.pcbi.1009149.
4. Müller SA, Paltra S, Rehmann J, Nagel K, Conrad TOF. Explicit modeling of antibody levels for infectious disease simulations in the context of SARS-CoV-2. *iScience*. 2023;26(9):107554. doi:10.1016/j.isci.2023.107554.
5. Kerkmann D, Korf S, Nguyen K, Abele D, Schengen A, Gerstein C, et al. Agent-based modeling for realistic reproduction of human mobility and contact behavior to evaluate test and isolation strategies in epidemic infectious disease spread. *Computers in Biology and Medicine*. 2025;193:110269. doi:10.1016/j.combiomed.2025.110269.

6. Radev ST, Graw F, Chen S, Mutters NT, Eichel VM, Bärnighausen T, et al. OutbreakFlow: Model-based Bayesian inference of disease outbreak dynamics with invertible neural networks and its application to the COVID-19 pandemics in Germany. *PLOS Computational Biology*. 2021;17(10):1–26. doi:10.1371/journal.pcbi.1009472.
7. Schmidt A, Zunker H, Heinlein A, Kühn MJ. Graph Neural Network Surrogates to leverage Mechanistic Expert Knowledge towards Reliable and Immediate Pandemic Response. *arXiv*. 2025;doi:10.48550/arXiv.2411.06500.
8. McMahan B, Moore E, Ramage D, Hampson S, Arcas BA. Communication-Efficient Learning of Deep Networks from Decentralized Data. In: Singh A, Zhu J, editors. *Proceedings of the 20th International Conference on Artificial Intelligence and Statistics*. vol. 54 of *Proceedings of Machine Learning Research*. PMLR; 2017. p. 1273–1282. Available from: <https://proceedings.mlr.press/v54/mcmahan17a.html>.
9. Rieke N, Hancox J, Li W, Milletari F, Roth HR, Albarqouni S, et al. The future of digital health with federated learning. *npj Digital Medicine*. 2020;3(1). doi:10.1038/s41746-020-00323-1.
10. Dayan I, Roth HR, Zhong A, Harouni A, Gentili A, Abidin AZ, et al. Federated learning for predicting clinical outcomes in patients with COVID-19. *Nature Medicine*. 2021;27(10):1735–1743. doi:10.1038/s41591-021-01506-3.
11. Fu C, Zhang X, Ji S, Chen J, Wu J, Guo S, et al. Label Inference Attacks Against Vertical Federated Learning. In: *31st USENIX Security Symposium (USENIX Security 22)*. Boston, MA: USENIX Association; 2022.
12. Li O, Sun J, Yang X, Gao W, Zhang H, Xie J, et al. Label leakage and protection in two-party split learning. *NeurIPS 2020 Workshop on Scalability, Privacy, and Security in Federated Learning (SpicyFL)*. 2020;doi:10.48550/arXiv.2102.08504.
13. Melis L, Song C, De Cristofaro E, Shmatikov V. Exploiting unintended feature leakage in collaborative learning. In: *2019 IEEE symposium on security and privacy (SP)*. IEEE; 2019. p. 691–706.
14. Nasr M, Shokri R, Houmansadr A. Comprehensive privacy analysis of deep learning: Passive and active white-box inference attacks against centralized and federated learning. In: *2019 IEEE symposium on security and privacy (SP)*. IEEE; 2019. p. 739–753.
15. Wainakh A, Ventola F, Müßig T, Keim J, Cordero CG, Zimmer E, et al. User-Level Label Leakage from Gradients in Federated Learning. *Proceedings on Privacy Enhancing Technologies*. 2022;2022(2):227–244. doi:10.48550/arXiv.2105.09369.
16. Zhao B, Mopuri KR, Bilal H. iDLG: Improved deep leakage from gradients. *arXiv preprint arXiv:200102610*. 2020;doi:10.48550/arXiv.2001.02610.
17. Zhu L, Liu Z, Han S. Deep leakage from gradients. *Advances in Neural Information Processing Systems*. 2019;32. doi:10.48550/arXiv.1906.08935.
18. Dwork C, McSherry F, Nissim K, Smith A. Calibrating noise to sensitivity in private data analysis. In: *Theory of Cryptography: Third Theory of Cryptography Conference, TCC 2006, New York, NY, USA, March 4-7, 2006. Proceedings 3*. Springer; 2006. p. 265–284.

19. Dwork C, Roth A, et al. The algorithmic foundations of differential privacy. *Foundations and Trends in Theoretical Computer Science*. 2014;9(3-4):211–407. doi:10.1561/0400000042.
20. Ficek J, Wang W, Chen H, Dagne G, Daley E. Differential privacy in health research: A scoping review. *Journal of the American Medical Informatics Association*. 2021;28(10):2269–2276. doi:10.1093/jamia/ocab135.
21. Kerkouche R, Acs G, Castelluccia C, Genevès P. Privacy-preserving and bandwidth-efficient federated learning: An application to in-hospital mortality prediction. In: *Proceedings of the conference on health, inference, and learning*; 2021. p. 25–35.
22. Rahimian S, Kerkouche R, Kurth I, Fritz M. Practical challenges in differentially-private federated survival analysis of medical data. In: *Conference on Health, Inference, and Learning*. PMLR; 2022. p. 411–425.
23. Ryu M, Kim Y, Kim K, Madduri RK. APPFL: Open-Source Software Framework for Privacy-Preserving Federated Learning. In: *2022 IEEE International Parallel and Distributed Processing Symposium Workshops (IPDPSW)*; 2022. p. 1074–1083.
24. Madduri R, Li Z, Nandi T, Kim K, Ryu M, Rodriguez A. Advances in Privacy Preserving Federated Learning to Realize a Truly Learning Healthcare System. In: *2024 IEEE 6th International Conference on Trust, Privacy and Security in Intelligent Systems, and Applications (TPS-ISA)*; 2024. p. 273–279.
25. Hauer ME, Santos-Lozada AR. Differential Privacy in the 2020 Census Will Distort COVID-19 Rates. *Socius*. 2021;7:2378023121994014. doi:10.1177/2378023121994014.
26. Wilson RC, Butters OW, Avraam D, Baker J, Tedds JA, Turner A, et al. DataSHIELD – New Directions and Dimensions. *Data Science Journal*. 2017;16(0). doi:10.5334/dsj-2017-021.
27. Peñalvo JL, Mertens E, Ademović E, Akgun S, Baltazar AL, Buonfrate D, et al. Unravelling data for rapid evidence-based response to COVID-19: a summary of the unCoVer protocol. *BMJ Open*. 2021;11(11):e055630. doi:10.1136/bmjopen-2021-055630.
28. Huth M, Garavito CA, Seep L, Cirera L, Saúte F, Sicuri E, et al. Federated difference-in-differences with multiple time periods in DataSHIELD. *iScience*. 2024;27(11):111025. doi:10.1016/j.isci.2024.111025.
29. Robert Koch-Institut. SARS-CoV-2 Infektionen in Deutschland; 2025. Available from: https://robert-koch-institut.github.io/SARS-CoV-2-Infektionen_in_Deutschland.
30. Dwork C, Smith A, Steinke T, Ullman J. Exposed! A Survey of Attacks on Private Data. *Annual Review of Statistics and Its Application*. 2017;4(Volume 4, 2017):61–84. doi:10.1146/annurev-statistics-060116-054123.
31. Ansel J, Yang E, He H, Gimelshein N, Jain A, Voznesensky M, et al. PyTorch 2: Faster Machine Learning Through Dynamic Python Bytecode Transformation and Graph Compilation. In: *29th ACM International Conference on Architectural Support for Programming Languages and Operating Systems, Volume 2 (ASPLOS '24)*. ACM; 2024. Available from: <https://pytorch.org/assets/pytorch2-2.pdf>.

32. Mironov I. Rényi differential privacy. In: 2017 IEEE 30th computer security foundations symposium (CSF). IEEE; 2017. p. 263–275.
33. Bicker J, Kerkmann D, Korf SA, Plötzke L, Schmieding R, Wendler AC, et al.. MEmilio v2.0.0 - A high performance Modular EpideMIcs simuLatION software;. Available from: <https://elib.dlr.de/213614/>.
34. Statistische Ämter des Bundes und der Länder. Bevölkerung nach Geschlecht und Altersgruppen (17) – Stichtag 31.12. – regionale Tiefe: Gemeinden; 2025. <https://www.regionalstatistik.de/genesis/online?operation=table&code=12411-02-03-5>.